

Density profile slope in Dwarfs and environment

A. Del Popolo¹

ABSTRACT

In the present paper, we study how the dark matter density profiles of dwarfs galaxies in the mass range $10^8 - 10^{10} M_{\odot}$ are modified by the interaction of the dwarf in study with the neighboring structures, and by changing baryon fraction in dwarfs. To this aim, we determine the density profiles of the quoted dwarfs by means of Del Popolo (2009) which takes into account the effect of tidal interaction with neighboring structures, those of ordered and random angular momentum, dynamical friction, response of dark matter halos to condensation of baryons, and effects produced by baryons presence. As already shown in Del Popolo (2009), the slope of density profile of inner halos flattens with decreasing halo mass and the profile is well approximated by a Burkert's profile. We then treat angular momentum generated by tidal torques and baryon fraction as a parameter in order to understand how the last influences the density profiles. The analysis shows that dwarfs who suffered a smaller tidal torquing (consequently having smaller angular momentum) are characterized by steeper profiles with respect to dwarfs subject to higher torque, and similarly dwarfs having a smaller baryons fraction have also steeper profiles than those having a larger baryon fraction. In the case tidal torquing is shut down and baryons are not present, the density profile is very well approximated by an Einasto profile, similarly to dwarfs obtained in dissipationless N-body simulations. We then apply the result of the previous analysis to the dark matter halo rotation curves of three different dwarfs, namely NGC 2976, known to have a flat inner core, NGC 5949 having a profile intermediate between a cored and a cuspy one, and NGC 5963 having a cuspy profile. After calculating baryon fraction, which is $\simeq 0.1$ for the three galaxies, we fitted the rotation curves changing the value of angular momentum. NGC 2976, has an higher value of ordered angular momentum ($\lambda \simeq 0.04$) with respect to NGC 5949 ($\lambda \simeq 0.025$) and in the case of NGC 5963 the very steep profile can be obtained with a low value of λ ($\lambda \simeq 0.02$) and also decreasing the value of the random angular momentum. In the case of NGC 2976 tidal interaction with M81 could have also influenced the inner part of the density profile.

¹Dipartimento di Fisica e Astronomia, Università di Catania, Viale Andrea Doria 6, 95125 Catania, Italy

Subject headings: cosmology: theory - large scale structure of universe - galaxies: formation

1. Introduction

Dwarf galaxies are the most diffused type of galaxies in the Universe and were probably even more numerous in the past, when they might have contributed to the population of blue systems overabundant in deep galaxy counts (e.g. Lyly et al. 1995; Peimbert and Torres-Peimbert 1974) and more likely to the assembling of larger baryon systems. In spite of having received less attention than spiral and elliptical galaxies, dwarf galaxies have probably more cosmological relevance. Dwarf galaxies provide opportunities for drawing inferences about the processes in the early universe by observing our cosmological backyard—the Local Group and its vicinity. One of the main cosmological interests is related to the possibility that today's dwarfs are the survivors of the building blocks of massive galaxies. In the standard picture dwarf galaxies, like giants, formed from the gravitational instability driving the dark matter (DM) to cluster hierarchically in a bottom-up fashion. Most of the dark halos that formed before reionization had masses smaller than $10^8 - 10^9 M_{\odot}$ (e.g., Gnedin & Ostriker 1997). The small mass halos that survived tidal destruction to the modern epoch, were able to form stars, and constitute a subpopulation of dwarf satellites orbiting larger halos. Small mass dark halos significantly outnumber more massive galaxies like the Milky Way and can be located in the voids between luminous galaxies (e.g., Hoeft et al. 2006; Ricotti 2009). Dwarf galaxies are characterized by low mass, low luminosity, low metallicity, and small size. A common property to all dwarf galaxies studied in sufficient detail so far is the presence of an old population (Grebel 2001). Morphologically, dwarf galaxies can be classified as dwarf spiral galaxies, blue compact dwarf galaxies (BCDs), dwarf irregular galaxies (dIrrs), dwarf elliptical galaxies (dEs), dwarf spheroidal galaxies (dSphs) and tidal dwarf galaxies.² The difference in the spatial distribution of dEs and dSphs on the one hand

²Dwarf spiral galaxies, BCDs and dIrrs are star-forming objects, gas rich, rotationally supported, but late-type dwarf spirals are slow rotators or exhibit solid-body rotation. Dwarf Spiral galaxies are found in clusters and in the field, BCDs are often observed in relative isolation away from the dense centers of clusters or groups, and dIrrs clusters, groups and in the field. dEs are the most populous type of dwarf galaxies (Ferguson & Binggeli 1994), they tend to be found close to massive galaxies, usually have little or no detectable gas, and are often not rotationally supported, similarly to dSphs. Tidal dwarf galaxies form from the debris torn out of more massive galaxies during interactions and mergers. In contrast to other dwarf galaxies they do not contain dark matter and may have high metallicities for their luminosity depending on

and dIrrs on the other hand is also known as morphological segregation or as the morphology-density relation for dwarf galaxies and may be a signature of environmental effects on galaxy evolution. While dwarf galaxies are of fundamental importance in cosmology, they continue to challenge our cosmological models and models of galaxy formation. Two well-known problems, to them connected, are the missing satellites problem (Klypin et al. 1999; Moore et al. 1999) and the cores versus cusps problem, (de Blok 2010), namely the discrepancy of observed and simulated density profiles in the inner kpc of the halo. For what concerns this last one, the first comparisons of the HI rotation curves of gas-rich dwarf galaxies with those predicted by CDM profiles presented in Moore (1994) and Flores and Primack (1994), showed that the dynamics of these galaxies are dominated by dark matter, and they are therefore thought to be good probes of its distribution. Both studies show that halos of these late-type dwarf galaxies are best characterized by an approximately constant-density core, concluding that the modeled small-scale properties of CDM are fundamentally incompatible with observations (Carignan & Beaulieu 1989; Lake, Schommer, and van Gorkom 1990; Jobin & Carignan 1990; Broeils 1990) of dwarf galaxies (Moore 1994). A solution to the problem was proposed by Navarro et al. (1996), who argued that a dark matter core can be created if a large fraction of the baryons is suddenly expelled into the halo, and Gelato and Sommer-Larsen (1999) reproduced the observed rotation curve of DDO 154 by simulating NFW halos, and subjecting them to the effect of violent gas outflows, which are simulated by suddenly changing the disk potential in the simulations. This kind of analysis are no longer in the realm of cosmology, but are dealing with “messy” astrophysics. However, there is an alternative way to study the dark matter distribution. Finding and investigating more massive dark-matter dominated galaxies, such as spiral galaxies, where the potential well is too deep to efficiently remove the gas, may therefore be a more effective way to explore the core/cusp issue. These galaxies are called Low Surface Brightness (LSB) galaxies, namely late-type, gas-rich, dark-matter-dominated disk galaxies. Their optical appearance is dominated by an exponential disk with a young, blue population, with little evidence for a dominant old population. Additionally, these galaxies do not have large dominant bulges.³ Also LSB galaxies seem to indicate that the shape of the density profile at small scales is significantly shallower than what is found in numerical simulations (e.g., de Blok, Bosma, and McGaugh 2003). The cusp/core problem is also observed in spheroidal galaxies. In fact, despite the

the evolutionary stage of the parent galaxy (Duc & Mirabel 1998).

³The type of LSB galaxies most commonly studied, in particular with regards to the core/cusp controversy, are the late type LSB galaxies whose properties are described previously. The other type of LSB galaxies often discussed in the literature is the massive, early-type, bulge-dominated LSB galaxies. These galaxies have properties entirely different from the late-type LSB galaxies (Pickering et al. 1997; Sprayberry et al. 1995).

inner structure of spheroidal galaxies is harder to determine, Kleyna et al. (2003), by means of N-body simulations, showed that Ursa Minor dSph would survive for less than 1 Gyr if the DM core were cusped. Additionally, Magorrian (2003) found $\alpha = 0.55^{+0.37}_{-0.33}$ for the Draco dSph. The largest part of studies of dwarf galaxies arrive at the conclusion that the inner part of density profiles is characterized by a core structure, and that cuspy profiles, even if not excluded are more rare than cores (Flores & Primak 1994; Moore 1994; Burkert 1995; Kravtsov et al. 1998; Salucci & Burkert 2000; Borriello & Salucci 2001; de Blok et al. 2001; de Blok & Bosma 2002; Marchesini et al. 2002; de Blok 2003; de Blok, Bosma & McGaugh 2003; Gentile et al. 2004, 2006; Simon et al. 2005 (hereafter S05); Spekkens et al. 2005; Oh et al. 2010). In particular Kravtsov et al. (1998) and de Blok, Bosma & McGaugh (2003) find that a halo model with a mildly cuspy slope $\alpha = -0.2 \pm 0.2$ gives the best description of the data in the presence of realistic observational effects, and Spekkens et al. (2005) found best-fitting slopes from $\alpha = -0.22 \pm 0.08$ to $\alpha = -0.28 \pm 0.06$, depending on how they select their sample. They also model pointing and slit offsets, and came to the conclusion that, after correction, their data are consistent with cuspy haloes. Swaters et al. (2003) also presented extensive modeling of high-resolution long-slit H α rotation curves, and showed that while their data are consistent with $\alpha = 0$ cores, steeper slopes cannot be ruled out. Similarly van den Bosch et al. (2000) who used the de Blok and McGaugh (1997) data, along with high-resolution literature rotation curves of a number of late-type “normal” and dwarf galaxies, such as DDO154 and NGC 247 concluded that the LSB galaxy HI data were consistent with both cored and cuspy halos. In their analysis of the other gas-rich dwarf and late-type galaxies, they found evidence for cores in the dwarf galaxies, but detected a steep mass-density slope consistent with a cusp in NGC 247. Hayashi et al. (2004) performed a direct comparison of the spherically averaged dark matter circular velocity profiles with H α rotation curves of a sample of low surface brightness (LSB) galaxies. They found that most galaxies in the sample (about 70 per cent) have rotation curves that are consistent with the structure of CDM haloes, namely they are consistent with steep slopes. High-resolution velocity fields led Blaise-Ouelette et al. (2004), Spanó et al. (2008) to conclude that the pseudo-isothermal sphere (PI) generally provided better fits than NFW models. Kuzio de Naray et al. (2008, 2009) presented DensePak velocity fields of LSB galaxies, many of them taken from the de Blok and McGaugh (1997) sample. Their conclusions are that NFW models provide a worse fit than PI models, for all values of the stellar mass-to-light ratio Υ_* . Oh et al. (2010) presented mass models for the dark matter component of seven dwarf galaxies (IC 2574, NGC 2366, Ho I, Ho II, DDO 53, DDO 154, M81dwB) taken from “The HI Nearby Galaxy Survey” (THINGS). They are better described by core-like models such as pseudo-isothermal halo models dominated by a central constant-density core. The mean value of the logarithmic inner slopes of the mass density profiles is $\alpha = -0.29 \pm 0.07$. Apart from some cases already reported (e.g., Hayashi et al. (2004) or Swaters et al. 2003), some

other observations have pointed out the fact, several times reported, that not all dwarfs are characterized by flat cores, but some of them have cuspy profiles. For example, S05 studied the inner slope of some dwarfs, namely NGC 2976, 4605, 5949, 5693, 6689. The full sample of these galaxies contains density profiles that span the range from $\alpha = 0$ (NGC 2976) to $\alpha = 1.28$ (NGC 5963), where α is the power-law index describing the central density profile. The scatter in α from galaxy to galaxy is 0.44, 3 times as large as in cold dark matter (CDM) simulations, and the mean density profile slope is $\alpha = 0.73$, shallower than that predicted by the simulations. Swaters et al. (2003) presented a DensePak velocity field of the late-type dwarf galaxy DDO 39. They derive a rotation curve, and show that its slope is steeper than implied by lower resolution HI data, and also different from earlier long-slit data from de Blok and Bosma (2002). For the dark matter halo, they considered a generalized NFW halo and obtained the result that fits to the uncorrected and pressure-corrected rotation curves (RCs) give virtually identical results, with best fits in the range $0 < \alpha \leq 0.8$. For the RC corrected using the virial theorem, best fits are found for somewhat steeper inner slopes, in the range $0.3 \leq \alpha \leq 1$. In a recent paper de Blok et al. (2008), by using the THINGS sample, found that for galaxies having $M_B < -19$ a NFW profile or an PI profile statistically fit equally well the density profiles of galaxies, while for $M_B > -19$ the core dominated PI model fits significantly better than the NFW model. In other terms, for low mass galaxies a core dominated halo is clearly preferred over a cusp-like halo, while for massive, disk dominated galaxies, the two models fit apparently equally well. The previous discussion pointed out that, although large part of the observations conclude that dwarfs have a core-like profile (e.g., de Blok, Bosma & McGaugh 2003), this does not imply that does not exist some dwarfs that have cuspy profiles (e.g., S05). The previous arguments lead to some important question: is there a correlation between the value of slope of galaxies tidally influenced by external galaxies and the tidal field? How much the baryons in the dwarf influence its final density profile? Since some studies (e.g., S05, de Blok et al. 2008) hint to a possible correlation between inner slope of dwarfs and their mass and interaction with neighbors, would be important to verify from a theoretical point of view if the quoted correlations are admissible. On the other hand, the morphology-density relation illustrates that environment is an important factor in dwarfs evolution. In the present paper, we analyze how different tidal torques and baryons content of haloes influence dwarfs density profile. The paper is organized as follows: in Section 2, we summarize the model used. In Section 3.1, we determine the dwarfs density profiles when tidal torques and baryons fraction is changed. In Section 3.2, we compare the previous results with three different galaxies, namely NGC 2976, NGC 5949, and NGC 5963, and we discuss why the three dwarfs have different profiles. Section 4 is devoted to discussions and conclusions.

2. Model

2.1. Summary of Del Popolo 2009 model

In the present study, the dwarfs galaxies dark matter haloes are formed using the analytical method introduced in Del Popolo (2009), which is summarized in the following. We added a discussion on the way baryon fraction was calculated, not present in Del Popolo (2009) (hereafter DP09).

Since the seminal paper by Gunn & Gott (1972), the spherical infall model has been extensively used in the literature. In the quoted model a bound mass shell of initial comoving radius x_i expands to a maximum radius x_m (named apapsis or turnaround radius x_{ta}). As successive shells expand to their maximum radius, they acquire angular momentum and then contract on orbits determined by the angular momentum. Dissipative physics and the process of violent relaxation will eventually intervene and convert the kinetic energy of collapse into random motions (virialization). Knowing the initial comoving radius x_i , the mean fractional density excess inside the shell, as measured at current epoch t_0 , assuming linear growth, namely $\bar{\delta}_i$, and the density parameter Ω_i , assuming that mass is conserved and that each shell is kept at its turn-around radius, one can easily obtain the shape of the density profile at turn-around, $\rho_{ta}(x_m)$ (Peebles 1980; Hoffman & Shaham 1985 (hereafter HS); White & Zaritsky 1992). The final density profile is obtained assuming that the potential well near the center varies adiabatically (Gunn 1977, FG84), which means that a shell near the center makes many oscillations before the potential changes significantly (Gunn 1977, FG84, Zaroubi & Hoffman 1993) and summing the contribution of the collapsing shells. The final density profile can be obtained in terms of the density at turn-around, $\rho_{ta}(x_m)$, the collapse factor⁴, and the turn-around radius (Eq. A18, DP 2009), as:

$$\rho(x) = \frac{\rho_{ta}(x_m)}{f^3} \left[1 + \frac{d \ln f}{d \ln x_m} \right]^{-1} \quad (1)$$

The model takes into account angular momentum, dynamical friction, and adiabatic contraction of dark matter. There are two sources of angular momentum of collisionless dark matter: (a) bulk streaming motions, and (b) random tangential motions. The first one (ordered angular momentum (Ryden & Gunn 1987 (RG87)), L , arises due to tidal torques, τ , exerted by a field of random density fluctuations on proto-halos (Hoyle 1953; Peebles 1969; White 1984; Ryden 1988; Eisenstein & Loeb 1995; Catelan & Theuns 1996). The tidal fields from the large-scale structure surrounding the proto-structure exert a torquing

⁴The collapse factor is defined as the $f = x/x_m$ (see DP09, Appendix A)

moment increasing the angular momentum of the system, which grows linearly in time prior to the gravitational collapse of the structure as proto-structures have large linear sizes, and thus, the surrounding material is able to imprint angular momentum efficiently. At later stages, after the protogalaxy decouples from the expanding background and turns around, the growth of angular momentum is reduced to a second order effect, because the collapse dramatically reduces the lever arms (Schaefer 2009). As described in RG87, to calculate the ordered angular momentum, one has first to obtain the rms torque, $\tau(r)$, on a mass shell and then calculate the total specific angular momentum, $h(r, \nu)$, acquired during expansion by integrating the torque over time (Ryden 1988a (hereafter R88), Eq. 35)

$$h(r, \nu) = \frac{1}{3} \left(\frac{3}{4} \right)^{2/3} \frac{\tau_o t_0 \bar{\delta}_o^{-5/2}}{M_{sh}} \int_0^\pi \frac{(1 - \cos \theta)^3}{(\vartheta - \sin \vartheta)^{4/3}} \frac{f_2(\vartheta)}{f_1(\vartheta) - f_2(\vartheta) \frac{\delta_o}{\delta_o}} d\vartheta \quad (2)$$

where $M_{sh} = 4\pi\rho_b [1 + \delta(x)] x^2 \delta x$ is the mass in a thin spherical shell of internal radius x , τ_o is the tidal torque at time t_0 , the functions $f_1(\vartheta)$, $f_2(\vartheta)$ are given by R88 (Eq. 31), $\delta_o = \frac{\rho - \rho_b}{\rho_b}$, ρ_b is the background density, $\bar{\delta}(r)$ is the mean overdensity inside the shell, and ν is the peak height (see DP09). As shown in DP09, the values obtained for angular momentum are in agreement with others studies (e.g. Catelan & Theuns 1996). The total angular momentum of a system is often expressed in terms of the dimensionless spin parameter

$$\lambda = \frac{L|E|^{1/2}}{GM^{5/2}}, \quad (3)$$

where L is the angular momentum, summed over shells, and E is the binding energy of the halo. The distributin of λ parameter is well described by a lognormal distribution (e.g. Vivitska et a. 2002). Using the parameters in Vivitska et al. (2002), the maximum of the distribution of λ is $\lambda = 0.035$, while there is a 90% probability that λ is in the range 0.02-0.1. The λ parameter shows a dependence on peak height (Catelan & Theuns 1996), cosmology, mass, and environment (Knebe & Power 2008; Cervantes-Sodi at al. 2008a,b). Cervantes-Sodi et al. (2008a, b) found a marked correlation of λ with mass, in the sense that low-mass galaxies present both higher mean values of λ and associated dispersions, than high-mass galaxies (see Fig. 5 of Cervantes-Sodi et al. 2008a; and Fig. 3 of Cervantes-Sodi et al. 2008b), while Cervantes-Sodi et al. (2010b) found a correlation between λ and cluster environment. So, while the baryons in bright disc galaxies seem to have spin parameters similar to those of their host haloes, dwarfs and LSB disc galaxies may tend to be associated with a higher spin parameter. For example, van den Bosch, Burkert & Swaters (2001, hereafter BBS) studied the spin in a sample of 14 low-mass disc galaxies with an estimated average of virial velocity $V \simeq 60$ km/s. They found an average spin parameter about 50% larger than that of the dark

haloes (see also Maller & Dekel 2002, Fig. 8 and Dekel & Woo 2003). Also Boissier et al. (2003), showed in their study that 35% of all galaxies (in number) with $0.06 < \lambda < 0.21$ are LSBs (see also Jimenez et al. 1998). According to several analytical papers (Nusser 2001; Hiotelis 2002; Le Delliou & Henriksen 2003; Ascasibar et al. 2004; Williams et al. 2004), one therefore expects that these high spin objects should typically have shallower density cusps⁵. Moreover the cores of these galaxies are also much less dense than the simulations indicate. The second one (random angular momentum (RG87)), j , is connected to random velocities (see RG87 and the following of the present paper), and was assigned to protostructures according to Avila-Reese et al. (1998) scheme as modified by Ascasibar et al. (2004) (see Appendix C2 of DP09). Note that Eq. (2) define the angular momentum profile $h(M)$. $h(M)$ is $\propto M^{1.3}$ similarly to Bullock et al. (2001). A wide discussion on both ordered (h) and random (j) angular momentum, with plots of the same (Figs. 7-9), is given in Del Popolo (2009) in Appendix C. Moreover, Fig. 2 in Del Popolo (2009) plots the distribution $P(J_{Tot}) - J_{Tot}$ of the total specific angular momentum.

Dynamical friction was taken into account as described in Antonuccio-Delogu & Colafrancesco (1994) (see also Appendix D of DP09). We also took into account adiabatic contraction (AC) of dark matter halos in response to the condensation of baryons in their centers, leading to a steepening of the dark matter density slope. Blumenthal et al. (1986) described an approximate analytical model to calculate the effects of AC. More recently Gnedin et al. (2004) proposed a simple modification of the Blumenthal model, which describes numerical results more accurately. For systems in which angular momentum is exchanged between baryons and dark matter (e.g., through dynamical friction), Klypin et al. (2002) introduced a modification to Blumenthal’s model. The adiabatic contraction was taken into account by means of Gnedin et al. (2004) model, and Klypin et al. (2002) model was used to take also account of exchange of angular momentum between baryons and dark matter. In Sect. 3.1, we describe how the baryon fraction, namely the ratio between the baryon mass and total mass was calculated and its adopted values. The result of our model (extensively described in DP09) shows that the structure of the inner density profiles is strongly influenced by baryon physics and exchange of angular momentum between baryons and dark matter. So, summarizing, in our analytical model the density profiles are:

- a) core-like when we take into account the presence of baryons and only in the inner part of the density profile. In the outer parts the result is the same of simulations.
- b) The results of dissipationless simulations, namely cuspy profiles, are re-obtained, with

⁵In contrast to relatively recently formed objects, such as clusters of galaxies, that present unrelaxed mass distributions, LSB galaxies with high central densities may have the highest formation redshifts, and therefore they have had almost a Hubble time to soften their cusps

very good accuracy, eliminating the baryons, not taken into account in dissipationless simulations. The results are in agreement with other models, e.g. Mashchenko et al (2005, 2006, 2007), Romano-Diaz et al. (2008), El-Zant et al. (2001), and Governato et al. (2010).

2.2. Baryon fraction

Baryon fraction was calculated as follows. Dwarf galaxies can be divided into gas-poor dwarf galaxies commonly known as dwarf spheroidal or dwarf elliptical galaxies, and as-rich dwarfs commonly known as dwarf irregular galaxies. Moreover, baryon content changes in the galaxy from the core to the outskirts (see Hoeft et al. 2006, Fig. 5). The universal baryon fraction, f_b , has been inferred by observations involving different physical processes (Turner 2002). The power spectrum of matter inhomogeneities in large-scale structure is sensitive to the quoted f_b ; the Two Degree Field Galaxy Redshift Survey reported a value of 0.15 ± 0.07 (Percival et al. 2001). Measurements of the angular power spectrum of the CMBR also provided a very significant estimate. The combined analysis in Jaffe et al. (2001) of several data sets gives $f_b = 0.186^{+0.010}_{-0.008}$. By using WMAP collaboration data (Spergel et al. 2003), one obtains $f_b \simeq 0.16$ ($\Omega_b = 0.047 \pm 0.006$; $\Omega_m = 0.29 \pm 0.07$). After baryons cool and form stars, the baryon-to-total mass at the virial radius does not need to equal the previous quoted universal baryon fraction and may deviate from it depending on feedback effects, hierarchical formation details, and heating by the extragalactic UVB flux. One has to take into account that for large galaxies, only about half of the baryons, in principle available within the virial radius, goes into the central galaxy. For dwarf galaxies, this amount may be much smaller because of feed-back effects, hierarchical formation details, and heating by the extragalactic UVB flux. Geha et al. (2006) studied the baryon content of low mass dwarf galaxies and Hoeft et al. (2006) studied structure formation in cosmological void regions investigating to which extent the cosmological UV-background reduces the baryon content of dwarf galaxies and in Hoeft & Gottlöber (2010) studied also the case of cosmological environment. As shown from McGaugh et al. (2010) (see their Fig. 2), the fraction of baryons detected in all forms deviates monotonically from the cosmic baryon fraction as a function of mass. On the largest scales of clusters, most of the expected baryons are detected, while in the smallest dwarf galaxies, fewer than 1% are detected. The detected baryon fraction is the ratio of the baryon fraction, $F_b = M_b/M_{500}$, and the universal baryon fraction, f_b :

$$f_d = (M_b/M_{500})/f_b = F_b/f_b \quad (4)$$

where M_{500} is the mass contained within a radius where the enclosed density is 500 times the critical density of the Universe, and the baryon mass $M_b = M_* + M_{gas}$, where M_* is the stellar mass and M_{gas} is that of gas. For example for a dwarf of $M_b = 2 \times 10^7 M_\odot$, with

$M_{500} = 2 \times 10^9 M_\odot$ (see Table 2 in McGaugh et al. 2010), f_d is $\simeq 0.04$, and the baryon fraction $F_b = M_b/M_{500} = 0.01$.

3. Results and discussion

3.1. Density profiles, torque and baryons fraction

Λ CDM models face a number of challenges on galactic scales (de Blok & McGaugh 1997; Flores & Primack 1994; Moore 1994; Ostriker & Steinhardt 2003). One of these in particular, the core/cusp problem, has persisted and been the subject of much discussion. In DP09, we showed how the flattening of the inner slopes of halos is produced by the role of angular momentum, dynamical friction, and the interplay between DM and baryon component. In particular, we studied the density profiles of haloes in the mass range $10^8 - 10^{15} M_\odot$. In the case of the dwarf galaxies mass range, the density profiles were core-like. As previously reported, in that study we moreover took into account the ordered angular momentum, due to tidal torques (see Eq. 2 and Section C of DP09), experienced by proto-halos in the neighborhood of the studied object. It would be then interesting to study the effects of different angular momenta and baryon fraction on the density profile of a given halo. So, in the following, using DP09, we will generate density profiles of haloes in the mass range $10^8 - 10^{10} M_\odot$ and we will study the effect of different ordered angular momentum and baryon fraction on the dwarf galaxy density profile. In a future paper, we also aim to study observationally the inner slopes of dwarfs who has no interacting companions, and those more close to parent galaxies. In Sect. 3.1, we use the baryons fraction of McGaugh et al. (2010). In Sect. 3.2, where we compare the results with three observed galaxies, we will discuss how the baryon fraction is chosen. The result of the calculation are shown in Fig. 1a, in which we plotted the density profiles of dwarfs with mass $10^8 M_\odot$ (dashed line), $10^9 M_\odot$ (dotted line), and $10^{10} M_\odot$ (solid line). This panel shows the results for haloes density profiles obtained in DP09 (which we will use as reference haloes). The angular momentum in Fig. 1a was obtained by the tidal torque theory as in DP09 and, in the case of the halo of $10^9 M_\odot$ has a value similar to UGC 7399 (see BBS), namely $h_* \simeq 400$ kpc km/s ($\lambda \simeq 0.04$). The baryon fraction ($f_{d_*} \simeq 0.04$)⁶ was fixed as described Sect. 2.2. The quoted plot shows flat density profiles well fitted by a Burkert profile, whose functional form is characterized by:

$$\rho(r) = \frac{\rho_o}{(1 + r/r_o)[1 + (r/r_o)^2]} \quad (5)$$

where $\rho_o \simeq \rho_s$ and $r_o \simeq r_s$ (El-Zant et al. 2001).

⁶Note that the “*” in f_{d_*} and in h_* does not “stand” for stellar, as in the case of M_*

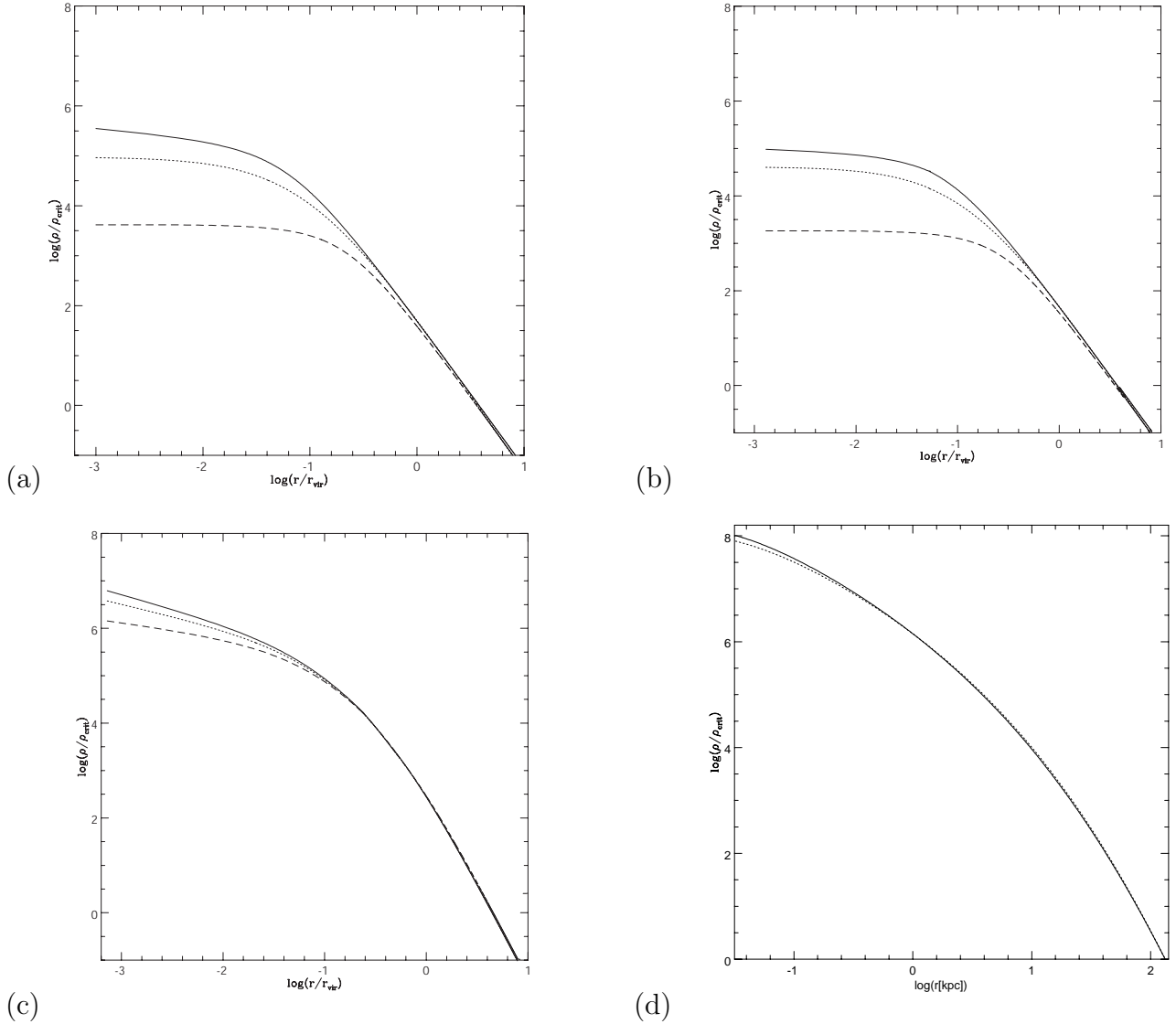


Fig. 1.— DM halos shape changes with angular momentum. DM haloes generated with the model of Section 2. In panels (a)(c), the dashed line, the dotted line and the solid line represent the density profile for a halo of $10^8 M_\odot$, $10^9 M_\odot$, and $10^{10} M_\odot$, respectively. In case (a), that is our reference case, the specific angular momentum was obtained using the tidal torque theory as described in DP09. The specific angular momentum for the halo of mass $10^9 M_\odot$ is $h_* \simeq 400$ kpc km/s ($\lambda \simeq 0.04$) and the baryon fraction $f_{d*} \simeq 0.04$. In panel (b) we increased the value of specific ordered angular momentum, h_* , to $2h_*$ leaving unmodified the baryon fraction to f_{d*} and in panel (c) the specific ordered angular momentum is $h_*/2$ and the baryon fraction equal to the previous cases, namely f_{d*} . Panel (d) shows the density profile of a halo of $10^{10} M_\odot$ with zero ordered angular momentum and no baryons (solid line), while the dashed line is the Einasto profile.

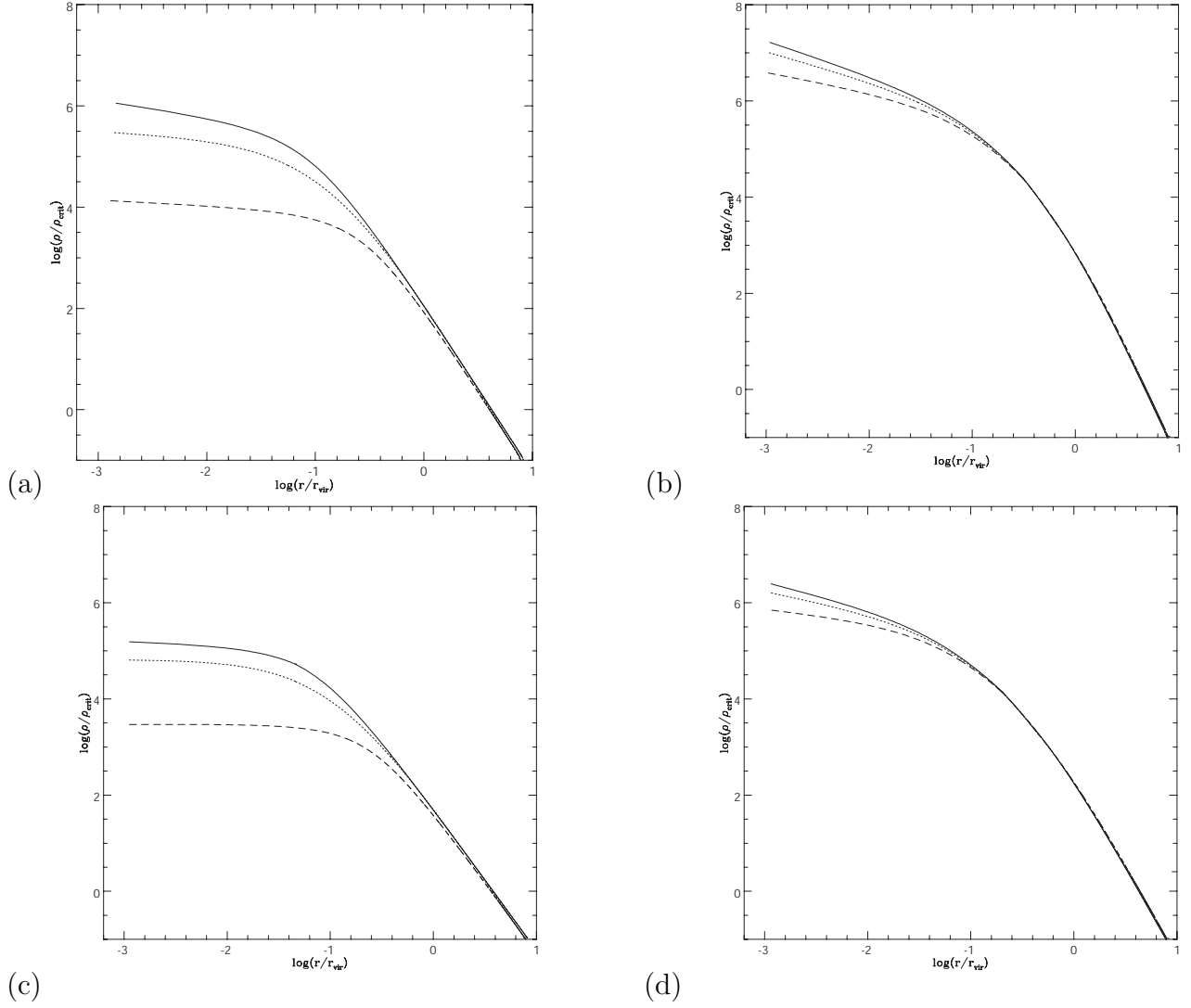


Fig. 2.— DM halos shape changes with baryon fraction. Same as previous figure, Fig. 1, but in panel (a) we reduced the value of baryon fraction of Fig. 1a (h_* , f_{d*}) to $f_{d*}/3$, and in panel (b) we reduced the value of baryon fraction of Fig. 1c to $f_{d*}/3$; in panel (c) we increased the value of baryon fraction of Fig. 1a ($h_*/2$, f_{d*}) to $3f_{d*}$, and in panel (d) we increased the value of baryon fraction of Fig. 1c to $3f_{d*}$.

A slight steepening of the density profile is visible in the case $10^{10}M_{\odot}$ in which case the inner slope of the profile is $\alpha \simeq 0.2$, while $\alpha \simeq 0$ for 10^8M_{\odot} - 10^9M_{\odot} . As previous discussed in Sect. 2, the ordered angular momentum acquired by proto-structures depends on mass and is higher for dwarf galaxies, moreover the values of λ has a range $\simeq 0.02 - 0.2$ (BBS; Boisier et al. 2003). So, after calculating the density profiles for value given by the tidal torque theory (TTT), we considered the effects of changing the values of ordered angular momentum in the range of the allowed values.

In Fig. 1b, we repeated the same calculation of panel (a) changing the amplitude of the ordered angular momentum (which is proportional to the tidal torque) to $2h_*$, leaving unchanged the baryon fraction to f_{d*} . In this case, the profiles are, as expected, flatter with respect to the reference case, and for the same mass as the reference case (10^8M_{\odot} , 10^9M_{\odot} , $10^{10}M_{\odot}$) the slope is $\alpha = 0$, in all three cases. In Fig. 1c, we plot the density profiles for haloes having a value of angular momentum $h_*/2$, (1/2 that of the reference case), leaving unchanged the value of baryon fraction to f_{d*} . In this case, the inner slope for haloes of the same mass (10^8M_{\odot} , 10^9M_{\odot} , $10^{10}M_{\odot}$) are, respectively, given by $\alpha \simeq 0.4$, $\alpha \simeq 0.5$, and $\alpha \simeq 0.6$. The previous results show a steepening of the slope with decreasing value of angular momentum, in agreement with several previous results (Sikivie et al. 1997; Avila-Reese et al. 1998; Nusser 2001; Hiotelis 2002; Le Delliou & Henriksen 2003; Ascasibar et al. 2004; Williams et al. 2004). The three panels show that: a) less massive haloes are less concentrated; b) the halo’s inner slope is smaller for smaller mass and higher angular momentum.

The first point can be explained as follows: higher peaks (larger ν), which are progenitors of more massive haloes (Peacock & Heavens 1990; Del Popolo & Gambera 1996, Gao & White 2007) have greater density contrast at their center, and so shells do not expand far before beginning to collapse. This reduces the angular momentum acquired and allows haloes to become more concentrated. Point (b) can be explained in a similar way to (a). Less massive objects are generated by peaks with smaller ν , which acquire more angular momentum (h and j). Angular momentum sets the shape of the density profile at the inner regions. For pure radial orbits, the core is dominated by particles from the outer shells. As the angular momentum increases, these particles remains closer to the maximum radius, resulting in a shallower density profile. Particles with smaller angular momentum will be able to enter the core but with a reduced radial velocity compared with the purely radial SIM. For some particles the angular momentum is so large that they will never fall into the core (their rotational kinetic energy makes them unbound). Summarizing, particles with larger angular momenta are prevented from coming close to the halo’s center and so contributing to the central density. This has the effect of flattening the density profile. Summarizing, larger ordered angular momentum (stronger interaction between the proto-dwarf and environment)

gives rise to flatter density profiles, while a larger value of mass produces an increase of the central density contrast, and a steeper profile. Fig. 1d shows the case of zero angular momentum and no baryons, for a halo of $10^{10}M_{\odot}$. The solid line is the result of the model of the present paper, while the dashed line is the Einasto profile, characterized by a logarithmic slope varying continuously with radius (Navarro et al. 2004, 2008), and having a functional form:

$$\ln(\rho/\rho_{-2}) = (-2/\eta)[(r/r_{-2})^{\eta} - 1] \quad (6)$$

where the characteristic radius, r_{-2} , is obtained by $d \ln \rho / d \log r = -2$, $\rho_{-2} \equiv \rho(r_{-2})$, and η is a free parameter, which for $\eta \sim 0.17$ reproduces fairly well the radial dependence of density profiles. In Fig. 1d, we did not add the plot of NFW profile since recent simulations (e.g., Navarro et al. 2004, Navarro et al. 2010) shows that density profiles from N-body simulations are better approximated by Einasto profiles. The correlation between steepness of density profiles and angular momentum is very important to have a better understanding of LSB galaxies. We recall that LSB galaxies are more angular-momentum-dominated than normal galaxies of the same luminosity (McGaugh & de Blok 1998; Boisier et al. 2003), implying a flatter density profile with respect to giant galaxies. Another parameter which influence the final density profile is the baryon content of the halo, namely the ratio of the baryon mass to the total mass. In the following, we will study how changes in baryon content affects the density profiles. To this aim, in Fig. 2a, we plotted the same density profiles of Fig. 1a but with a baryon fraction $f_{d*}/3$, and the value of specific angular momentum as left unchanged to h_* . The effect of reducing the baryon content has the effect of steepening the density profiles, with respect to the reference case. The inner slope for haloes having the same mass as the reference case (10^8M_{\odot} , 10^9M_{\odot} , $10^{10}M_{\odot}$) are, respectively, given by $\alpha \simeq 0.13$, $\alpha \simeq 0.16$, and $\alpha \simeq 0.32$. Fig. 2b represents the haloes of Fig. 1c ($h_*/2$, f_{d*}) but reducing the baryon fraction to $f_{d*}/3$. The inner slope are steeper than the one seen in Fig. 1c, namely we have $\alpha \simeq 0.4$, $\alpha \simeq 0.6$, and $\alpha \simeq 0.7$. Fig. 2c represents the same density profiles in Fig. 1a (h_* , f_{d*}) but in this case the baryon fraction is larger, namely $3f_{d*}$. Fig. 2d represents the same density profiles in Fig. 1c ($h_*/2$, f_{d*}) but in this case the baryon fraction is larger, namely $3f_{d*}$. A larger amount of baryons imply a flattening of the density profiles. Fig. 2c shows density profiles with $\alpha \simeq 0$, for the three previous mass values, and Fig. 2d shows density profiles with $\alpha \simeq 0.3$, $\alpha \simeq 0.45$, and $\alpha \simeq 0.51$. The tendency to have flatter profiles with increasing baryon content and shallower with larger baryon content is due to the fact that when more baryons are present the energy and angular momentum transfer from baryons to DM is larger and DM moves on larger orbits reducing the inner density.

3.2. Comparison with observed galaxies

In the following, we use mass models for the dark matter component of different dwarf galaxies, from a dwarf with flat inner profile (NGC 2976), to an intermediate one (NGC 5949) to one with a steep profile (NGC 5963) and compare these with those obtained from the model of Sect. 2.

3.2.1. NGC 2976

In Figs. 3a-b, we apply the model of Sect. 2 to find density profiles, as done in sect. 3.1, that we then compare to the minimum disk and maximum disk rotation curve of NGC 2976, respectively. Before, we summarize the characteristics of the quoted dwarf described in Simon et al. (2003) (hereafter S03). NGC 2976 is a regular Sc dwarf galaxy located in the M81 group having an absolute magnitudes of $M_B = -17.0$ and $M_K = -20.2$, and a total mass of $3.5 \times 10^9 M_\odot$ (measured at 2.2 kpc). In optical and near-infrared images it is clear that NGC 2976 is a bulgeless, unbarred, pure disk system (see Fig. 1 of S03) whose only relevant reservoirs of baryons to consider are the stellar and gaseous disks. For what concerns the stellar disk the average predicted values are $0.48 \pm 0.02 M_\odot / L_{\odot K}$ in K band and $1.07 \pm 0.07 M_\odot / L_{\odot R}$ in R band (S03). NGC 2976 has a molecular and atomic gas disk (the second has mass of $1.5 \times 10^8 M_\odot$, Appleton, Davies, & Stephenson 1981; Stil & Israel 2002) which do not contribute appreciably to its measured rotation curve. The kinematics of the gaseous disk is highly complex, exhibiting large non-circular motions near the center which could be the reflection of a triaxial halo (Kazantzidis et al. 2010). In Fig. 3a, the black circles with error-bars represent the minimum disk rotation curve obtained by S03. The rotation curve has a power-law behavior from the center to $r \simeq 110''$ (1.84 kpc) (solid line in Fig. 3a) whose corresponding dark matter profile can be fitted by $\rho_{tot} = 1.6(r/1pc)^{-0.27 \pm 0.09} M_\odot / pc^3$, representing the total (baryon plus dark matter) density profile. In Fig. 3a, the dashed line represents the result of the model of section 2 considering the total mass (sum of dark matter and baryons) (note that this is the only case in the paper where we plot the total mass: dark matter and baryons in order to compare results with the minimum disc rotation curve of S03), using $\lambda \simeq 0.04$, compatible with the value of λ given in Munõz-Mateos et al. (2011). The baryon fraction as calculated as follows. The baryon fraction in the case of NGC 2976 could be obtained as $(M_{gas} + M_*) / M_{tot}$, where $M_{tot} = 3.7 \times 10^9 M_\odot$ (S03), $M_{gas} = 1.5 \times 10^8 M_\odot$ (5% of the total mass) and $M_* = 5 \times 10^8 M_\odot$ (14% of the total mass) (S03). However, the values of the mass given refers only to the inner 2.2 kpc of the dwarf, so the quoted ratio would give just the baryon fraction of the inner part of the dwarf. For NGC 2976 as also for NGC 5949, and NGC 5963 there is not enough data to determine the

total mass and then the baryon fraction, since the dark matter halo is vastly more extended than any of the baryon tracers that are needed to measure the mass. So, one has to make a series of very broad assumptions, as done in McGaugh et al. (2010). In the case of NGC 2976, we know the inner masses and the circular velocity $V_c \simeq 75$ km/s. Governato et al. (2007) simulated a disk galaxy with $V_c = 70$ km/s and found that it has a virial mass of $1.6 \times 10^{11} M_\odot$, similarly to Kaufmann et al. (2007), who simulated galaxies with $V_c = 74$ km/s getting $M_{vir} = 1.1 \times 10^{11} M_\odot$. So, as for Fig. 1, 2, we shall use McGaugh estimates, taking account of the known rotation circular velocity of NGC 2976 and the simulated mass in Governato et al. (2007). This gives a value $f_d \simeq 0.1$. The plot shows that, on the entire length of the data, the model of this paper gives a very good fit to the rotation curve, better than NFW model and the power-law fit. The shape of the density profile of the dark matter halo (Fig. 3b), was obtained by S05 removing the rotational velocities contributed by the baryon components of the galaxy. As first step, the stellar disk is scaled as high as the observed rotation velocities allow (see also Fig. 10 of S03), obtaining a maximum disk having a mass-to-light ratio of $0.19 M_\odot / L_{\odot,K}$. Then subtracting the rotation velocities due to the stars, the rotation velocities due to the HI, and the rotation velocities due to the H2 in quadrature from the observed rotation curve, one obtains the dark matter density profile of the maximal disk:

$$\rho_{DM} = 0.1(r/1pc)^{-0.01 \pm 0.13} M_\odot / pc^3 \quad (7)$$

In Fig. 3b, the black circles with error-bars represent the dark matter rotation velocities for the maximal disk, and the solid line is a power-law fit to the halo velocities (for $14'' < r < 105''$). The slope of the total density profile of the galaxy ($\alpha_{DM} \leq 0.27 \pm 0.09$) represents the absolute upper limit for the slope of the dark matter density profile. This profile is composed of dark matter stars and gas, so the upper limit must be lower. Excluding strong and very young starburst, S05 concluded that the dark matter density profile is bracketed by $\rho_{DM} = r^{-0.17 \pm 0.09}$ and $\rho_{DM} = r^0$. In Fig. 3b, the dashed line represents again the result of the model of section 2, now considering only dark matter. Also in this case, the model of this paper gives a very good fit to the rotation curve, better than NFW model and the power-law fit. In the previous discussion, we saw that the density profile of NGC 2976 is very shallow, $\rho_{DM} = 0.1(r/1pc)^{-0.01 \pm 0.13} M_\odot / pc^3$, compatible with some results in literature (e.g., de Blok et al. 2003), but in contradiction with the N-body simulations results (Stadel et al. 2009 found a minimum value of the slope $\alpha = -0.8$ at 120 pc). As discussed by several papers (e.g. DP09; Governato et al. 2010), the shallow central density profile of NGC 2976 does not necessarily imply a problem for CDM model. Here, we only recall that one reason for the discrepancy between simulations and observations is due to the fact that simulations neglect the effects of the baryons on the dark matter halo. In the case of NGC 2976, the baryon mass dominates the central 220 pc of the galaxy even for the lower limit to mass-to-light ratio, and in the case of the maximal disk ($0.19 M_\odot / L_{\odot,K}$), the disk dominates out to a radius of 550

pc. So, summarizing, the flat density profile of NGC 2976 is produced, as discussed in DP09 by the role of angular momentum, dynamical friction, and the interplay between DM and baryon component. The importance of tidal torques in shaping dwarf galaxies density profile has been also suggested by the work of Stoehr et al. (2002) and Hayashi et al. (2003). These authors find in their simulations that dark matter satellite halos orbiting in the potential of a more massive neighbor are subject to tidal stripping. Although tides preferentially strip mass from the outer regions, tides also cause the halo to expand and the central density to decrease after each peri-centric passage. So, even if the effect of tidal field is more evident in the outer part of the dwarf also the inner profiles is influenced and it is shallower than their original profiles. However, tidal stirring is more efficient in forming dwarf spheroidal (dSph) galaxies starting from progenitors that are late type dwarfs affected by tidal forces (Kazantzidis et al. 2010, Lokas et al. 2010, Sales et al. 2010). If NGC 2976 can be identified with one of the most massive few dark matter satellites of M81, the quoted mechanism would have some effects on the shallowing of the density profile of the dwarf. Nowadays, NGC 2976 does not appear to be participating in the tidal interaction currently taking place between M81, M82, and NGC 3077 (Yun, Ho, & Lo 1994). Assuming that M81 has a total mass of $10^{12}M_{\odot}$ (Karachentsev et al. 2002), its tidal field only becomes comparable to the gravity of NGC 2976 (at a radius of 2 kpc) if the galaxies approach within 20 kpc of each other. Since M81 is currently at a projected distance of 79 kpc, the present-day kinematics of NGC 2976 are probably unaffected by the interaction, but nevertheless, the optical galaxy and the inner HI disk (Stil & Israel 2002a, 2002b) both appear regular, symmetric, and undisturbed, it has likely interacted with M81 in the past. Appleton et al. (1981) discovered a faint HI streamer stretching from M81 to NGC 2976, implying an interaction between the two objects. Boyce et al. (2001) used HIJASS data to show that this gas comprises a single tidal bridge that smoothly connects the two galaxies (see their Fig. 2a). The bridge contains somewhat more HI than NGC 2976 itself ($2.1 \times 10^8M_{\odot}$ and $1.5 \times 10^8M_{\odot}$, respectively). In summary, after the proto-structure decouples from the expanding background and turns around the growth of angular momentum is reduced to a second order effect, but later interactions (e.g., the one between M31 and NGC 2976) have an important role in the overall evolution of the total angular momentum of the protostructure, as shown by the results obtained from interacting systems, where the spin is visibly perturbed by the presence of a nearby companion. Tidal interaction of a dwarf with a neighbor in later phase of evolution of the dwarfs can increase (but see also Cervantes-Sodi 2010a) the effects of tidal torquing in the phase of proto-dwarf which furnish the angular momentum to the dwarf itself. In the present paper, we did not considered the tidal interaction among M31 and NGC 2976, which would further shallow its density profile.

3.2.2. NGC 5963 and NGC 5949

In Figs. 4a, b, we studied two other galaxies, NGC 5963 and NGC 5949. NGC 5963 is an Sc galaxy ($M_B = -17.8$ and mass of $1.4 \times 10^{10} M_\odot$) associated with the NGC 5866 group (Fouqué et al. 1992). The nearest large galaxy in the group is NGC 5907, at a projected distance of 430 kpc, so it is unlikely that NGC 5963 is currently interacting with its neighbors. The luminous component of NGC 5963 does not contain an easily identifiable exponential disk. At the center of the galaxy there is a bright, elongated, bar-like feature, and outside there is a small disk-like region (500 pc in radius). At a radius of 15" (950 pc) the surface brightness profile begins a steep decline, falling by nearly 3 mag over 18". Surrounding this region is an LSB, nearly exponential disk that extends out to a radius of at least 120". It is difficult to interpret NGC 5963 surface brightness profile in terms of the standard model of a disk galaxy. Ordinarily, one might assume that the bright central region of NGC 5963 is a bulge that just happens to be at the center of an unusually faint disk or that this structure is a pseudo-bulge that has formed via secular evolution of the galaxy (e.g., Kormendy & Kennicutt 2004). NGC 5963 also contains noncircular motions. NGC 5949 is a SBc galaxy ($M_B = -18.2$, $M \simeq 10^{10} M_\odot$). The surface brightness profiles of NGC 5949 are very similar to those of NGC 2976 (S03). Both galaxies contain a nucleus, a shallow (large scale length) inner disk, and a steep (small scale length) outer disk. The procedure to obtain rotation curves and dark matter density profiles of the two dwarfs is the same to that of NGC 2976 (S03). The limits placed by S05 on α_{DM} are $\alpha_{DM} = 0.79 \pm 0.17$, $\alpha_{DM} = 0.93 \pm 0.04$ for the maximum and minimum disk of NGC 5949 and $\alpha_{DM} = 0.75 \pm 0.10$, $\alpha_{DM} = 1.41 \pm 0.03$ for the maximum and minimum disk of NGC 5963. The dark matter density profile slopes derived after subtracting the stellar disks are $\alpha_{DM} = 0.88$ for NGC 5949, and $\alpha_{DM} = 1.20$ for NGC 5963, respectively. In Fig. 4a, the black points are the dark matter halo rotation curve of NGC 5963 after subtracting the stellar disk ($M_*/L_R = 1.24 M_\odot/L_{\odot,R}$). The thick green, the dotted cyan, the short-dashed magenta, and the long-dashed yellow curves show power-law, NFW, pseudo-isothermal, and the curve obtained from the model in the present paper, fits to the halo rotation curve, respectively. NGC 5963 quite clearly has a very steep central density profile. A power law with a slope of $\alpha_{DM} = 1.20$ fits the rotation curve very well, and an NFW fit with $r_s \simeq 11$ kpc and a concentration parameter of 14.9 is nearly as good. A pseudo-isothermal fit is significantly inferior⁷. The long-dashed yellow curve obtained with the model of this paper is an excellent fit. In order to obtain the quoted good fit, inside $\simeq 100$ pc we not also had to reduce the magnitude of h but also that of random angular momentum, j , (similarly to what done in Williams et al. 2004). In fact, as shown in Fig.

⁷Differently from Fig. 1d, in Fig. 4a,b we compared the results to the NFW profile to be consistent with S05, who compared his rotation curves to the NFW profile.

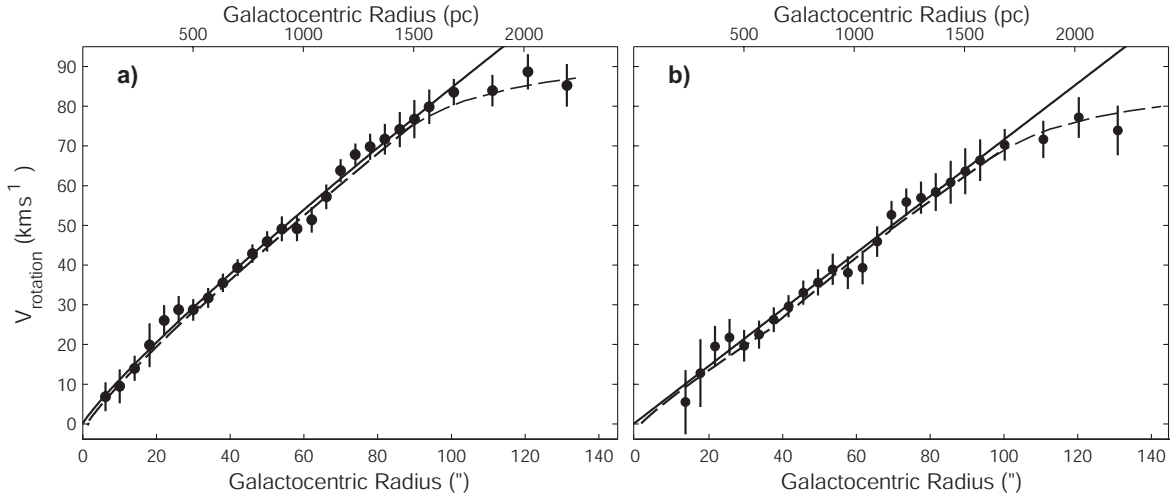


Fig. 3.— Panel (a). Minimum disk rotation curve of NGC 2976. Black circles with error-bars represent the rotation velocities relative to the minimum disk obtained by S03. The solid line is a power-law fit to the rotation curve characterized by $\rho \propto r^{-0.27}$. The dashed line plots the result of the model of the present paper. (b) Maximum disk rotation curve of NGC 2976. The dark matter rotation velocities are displayed as black circles with error-bars, as obtained by S03. The solid black curve is a power-law fit to the halo velocities (for $14'' < r < 105''$), which corresponds to a density profile of $\rho \propto r^{-0.01}$. The dashed line is again the result of the model of the present paper.

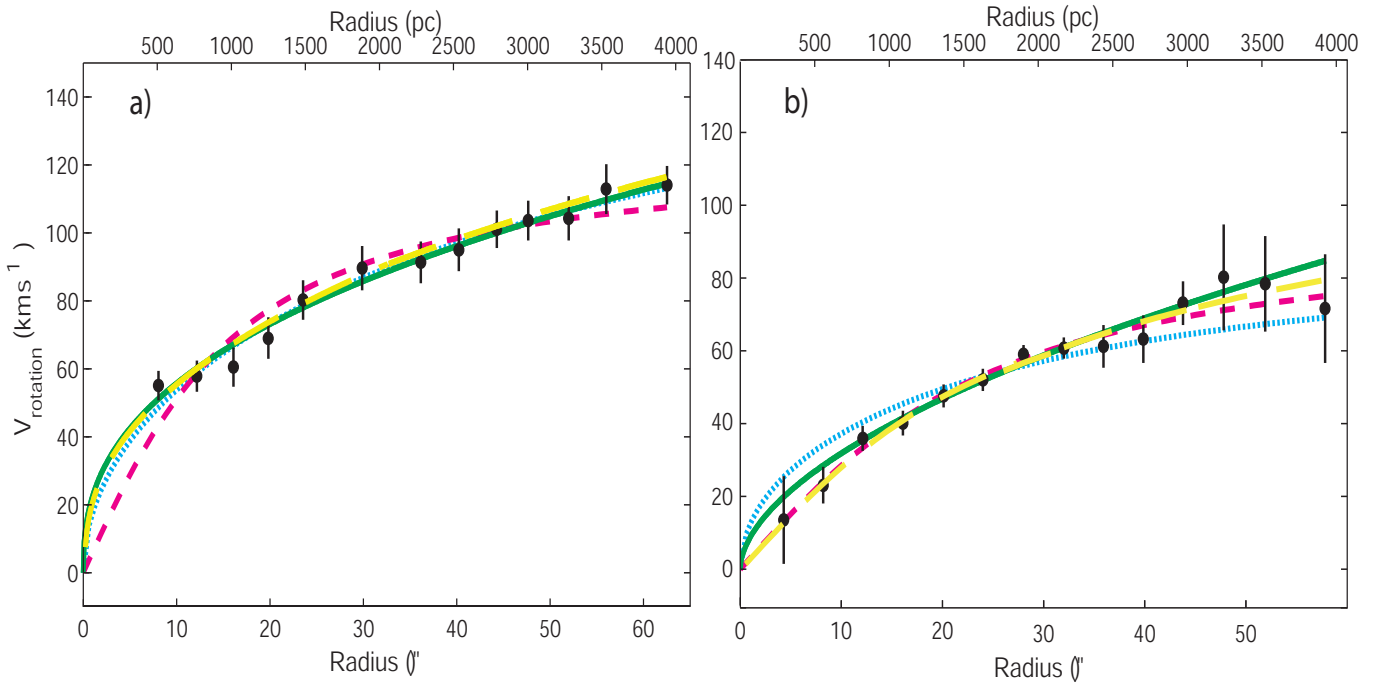


Fig. 4.— Panel (a). Disk-subtracted rotation curve of NGC 5963 (for $M_*/L_R = 1.24M_\odot/L_{\odot,R}$). The black points are the dark matter halo rotation curve after subtracting the stellar disk. The thick green, the dotted cyan, the short-dashed magenta, and the long-dashed yellow curves show, respectively, the power-law, NFW, pseudo-isothermal, and the curve obtained from the model in the present paper, fits to the halo rotation curve, respectively. Panel (b). Disk-subtracted rotation curve of NGC 5949 (for $M_*/L_R = 1.64M_\odot/L_{\odot,R}$). Symbols are as in panel (a).

1d, one obtain the steepest slope in the case the proto-structure is characterized by $h = 0$ and baryon fraction $F_b = 0$, as in dissipationless N-body simulations. The density profile is approximated by an Einasto profile. This last has a slope of $\simeq -0.8$ at $\simeq 100$ pc and $\simeq -1.4$ and at $\simeq 1$ kpc. If the proto-structure contains baryons and the ordered angular momentum is not zero the density profile will be flatter (as seen in Fig. 1, and Fig. 2). In the case of NGC 5963, the baryon fraction is obtained as in the case of NGC 2976, by means of Mcgaugh et al. (2010), for an objet having $V_c \simeq 120$ km/s, and is given by $f_d \simeq 0.12$. As always reported, a good fit to NGC 5963, is obtained with a value of specific angular momentum $h_*/2$ and reducing the random angular momentum j to $j/2$ (see Fig. 6 of Williams et al. 2004), which steepens the density profile. In Fig. 4b, we plot the disk-subtracted rotation curve of NGC 5949 (for $M_*/L_R = 1.64M_\odot/L_{\odot,R}$). Symbols are as in panel Fig. 4a. NFW fits to the disk subtracted rotation curve can be carried out, but the fit parameters are not usefully constrained. NGC 5949 is best fit by a PI density profile, but power laws with slopes slightly shallower than NFW ($\alpha_{DM} = 0.88$), and the modified pseudo-isothermal profile of equation:

$$\rho = \frac{\rho_c}{(r/r_c)^{1/2}(1 + r/r_c)^{3/2}} \quad (8)$$

where r_c and ρ_c are the characteristic radius and density, respectively, fit very well. The long-dashed yellow curve obtained with the model of this paper is an excellent fit. In this case, $V_c \simeq 80$ km/s, and $f_d \simeq 0.1$ and the value of specific ordered angular momentum $h_*/1.6$. Before going on, we want to recall that S03 and S05 analyses method differs in a few aspects from the other precedent cited studies. Firstly, their inner slope values are derived from a single power law fit to the entire rotation curve. Secondly, most of their models do not take into account the gas component due to a lack of HI observations. In the galaxies that they studied, however, the stellar disk almost always contributes significantly more mass at the center of the galaxy than the gas does, and the effect of including the gas is similar to a 20% change in the stellar mass-to-light ratio (Bolatto et al. 2002; S03). Arbitrarily increasing the stellar mass-to-light ratio (M_*/L) to simulate this effect, the slope of the dark matter density profile decreases by 2%-12%. Allowing the stellar disk to have a nonzero thickness (see section 2.2 of S05) would offset this decrease.

Finally, I would like to add that the same kind of processes operating in the late-type dwarfs that we previously discussed take place in LSBs, and that LSBs case was already studied in DP09 (Fig. 4).

3.2.3. Explaining the differences

The quoted examples show that not all dwarfs are characterized by flat inner cores (like NGC 2976), some have intermediate slopes between pseudo-isothermal profiles and NFW profiles (NGC 5949) other are well fitted by NFW profile (NGC 5963). One question we could ask is: why NGC 5949, NGC 5963 (and also NGC 4605; NGC 6689) have steeper inner profiles, in some case (NGC 5963) compatible with the NFW model? In Sect. 3.1, we have seen how larger values of the baryons fraction and tidal interaction with neighbors produces flatter profiles. However, Fig. 1 and Fig. 2 show that increases in angular momentum has a role more important than increase in baryon fraction (increase of a factor 2 in angular momentum produces similar effects than increase of a factor 3 in baryon fraction). For what concerns baryon fraction, the baryon fraction in the case of NGC 5963 is $f_d \sim 0.12$ and it is similar in the case of the other two galaxies (NGC 2976, NGC 5949). One should take into account that it is not only important if the baryons fraction is similar for different dwarfs (as in the case of NGC 2976, NGC 5949, NGC 5963) to have similar density profiles (all the rest being the same), but is very important how it is distributed in the galaxy (e.g., Hoeft et al. 2006, show in their figure 5 how the baryons fractions can strongly change going from the center to the outskirts of the dwarf). Now, the inner baryon fraction of NGC 2976 and NGC 5963 (using S03, S05 data and Bosma et al. 1988 data), at 2 kpc are similar, and of the order of f_b . This very high inner baryon fraction are due to a funneling of baryons toward the center of the dwarfs. In fact, in the case of NGC 2976, Williams et al. (2010) found similar ancient populations at all radii but significantly different young populations at increasing radii. In particular, outside of a well-measured break in the disk surface brightness profile, the age of the youngest population increases with distance from the galaxy center, suggesting that star formation is shutting down from the outside-in. The current rate and gas density suggest that rapid star formation in NGC 2976 is currently in the process of ceasing from the outside-in due to gas depletion. This process of outer disk gas depletion and inner disk star formation was likely triggered by an interaction with the core of the M81 group ≥ 1 Gyr ago that stripped the gas from the galaxy halo and/or triggered gas inflow from the outer disk toward the galaxy center (Williams et al. 2010). So, in NGC 2976, the funneling of baryons toward the central region produces a larger exchange of angular momentum through baryons and dark matter and an inner flatter profile with respect to other dwarfs. We know that the surface brightness profile of NGC 5949 is very similar to that of NGC 2976, and probably it has similar inner baryon fraction of NGC 2976. For what concerns NGC 5963, differently from the other galaxies it has a sharp transition between the inner and outer surface brightness profiles. This causes the derived stellar disk rotation curve to peak at small radii ($r = 20''$) and then drop steeply, making the outer parts of the galaxy highly dark matter dominated (see Fig. 6b of S05). As previously discussed, the

galaxy could contain a pseudo-bulge, and so like in NGC 2976 some process have funneled baryons toward the center of the galaxy. This means that in the case of these three dwarfs the baryon fraction is playing a similar role in shaping the density profile. According to our model, another factor in shaping density profile is the mass of the dwarf. Among the galaxies studied by S05, namely NGC 2976, NGC 4605, NGC 5949, NGC 5963, and NGC 6689, NGC 5963 has the highest central surface brightness. It also has the most unusual surface brightness profile (see S05, sect. 3.5.3). NGC 5963 is at the brighter end of the luminosity range of the quoted galaxies ($M_I = -19.1$), It does have the highest mass, in the sample. From the point of view of our model, a larger mass imply a steeper profile (however in the case of NGC 5963, NGC 5949, and NGC 2976 this difference is very small (see Table 7 of S05). Also in a recent paper de Blok et al. (2008), by using the THINGS sample, showed that in smaller objects core dominated halo is clearly preferred over a cusp-like halo, while for massive, disk dominated galaxies, PI and NFW fit apparently equally well. In other terms, for low mass galaxies a core dominated halo is clearly preferred over a cusp-like halo, while for massive, disk dominated galaxies, all halo models fit apparently equally well. This because more massive galaxies tend to have a more compact light-distribution, and therefore a more compact stellar mass distribution as well. This makes the contribution of the disk to the inner rotation curve critically dependent on the stellar mass-to-light ratio, and the initial mass function (IMF). So one could imagine a situation where the M/L_* could be changed to produce flat profiles for massive galaxies, and these changes do not have to be very large. Low mass galaxies have instead a reduced sensitivity to the M/L_* values, implying that changes of the quoted ratio does not influence the profile shape.

For what concerns, the role of tidal torques, we know that in the case of NGC 2976 we need a higher value of the specific angular momentum (h , $\lambda = 0.04$) than in the case of NGC 5963 and NGC 5949 to fit the profile. Tidal torques influence not only dwarfs during their formation, but if the environment contains close galaxies, tidal torques can influence the shape of the density profile. A search in NED (Nasa Extragalactic Database), concerning NCG5963 and the other quoted galaxies, gives to us the following results: as previously reported, NGC 2976 is a satellite of M81, NGC 5949 closest neighbor is a dwarf galaxy 300 kpc away. NGC 5963 is part of a small group; the closest neighbor is a dwarf galaxy 200 kpc away, and the massive galaxy NGC 5907 ($3 \times 10^{10} M_\odot$, Lequeux et al. 1998) is about 400 kpc away. So, NGC 5963 is the only other galaxy that could be regarded as having a similar environment to NGC 2976, even if the actual projected distance between M81 and NGC 2976 is 79 kpc and in the case of NGC 5963 the neighbors are at a much larger distance, and moreover although for NGC 2976 there is good evidence that it has interacted with M81, there is not really significant evidence for an interaction between NGC 5963 and its

neighbors⁸. In other terms the galaxy can be considered isolated and, as seen in Sect. 3.2, this imply that one cannot expect flattening of the density profile by tidal interactions, like for NGC 2976. Similar conclusions are valid for NGC 5949. Differently, in the case of NGC 2976, the interaction with M81 further contributed to the flattening of the density profile. Karachentsev & Kashibadze (2006) in their study of the masses of the Local Group and of the M81 group, obtained by distortions in the local velocity field, introduced the so-called tidal or galactic isolation index, TI, whose negative values correspond to isolated⁹ galaxies of the general field and positive values to members of the groups. In the case of NGC 2976, we have $TI = 2.7$, indicating that the galaxy is non-isolated, and as previously seen its inner slope has $\alpha \simeq 0.01$. In the case of NGC 4605, we have $TI = -1.1$, indicating that the galaxy is isolated, and the inner slope is steeper ($\alpha \simeq 0.78$). Several other similar example are possible, showing flat profiles for non-isolated dwarfs. In the case of NGC 2366, we have $TI = 1$, indicating that the galaxy is non-isolated, and the inner slope is $\alpha \simeq 0.12$ (Oh et al. 2010). As reported in the introduction, one of the most recent studies on mass modeling for dark matter component of galaxies is the work of Oh et al. (2010), in which all the seven dwarfs chosen from THINGS are better described by core-like models. However, we want to point out that at least 5 of the quoted dwarfs are characterized by a positive TI, namely NGC 2366 ($T = 1$), ICG2574 ($T = 0.9$), HoII ($T = 0.6$), DDO53 ($T = 0.7$), HOI ($T = 1.5$), indicating that the objects are non-isolated, and one should expect flat profiles, as observed. It would be interesting to extend the previous set of Oh to include isolated objects and to compare the density profile of the last with those of non-isolated dwarfs. The quoted example and the discussion of the previous sections, indicates that tidal interaction, baryon fraction, and environmental effects, influence the slope of the dwarfs density profile. This is not unexpected, since we know that on the other hand, the morphology-density relation illustrates that environment is an important factor. The existence of a correlation between galaxy morphology and local density environment (Dressler 1980, Goto et al. 2003, Park et al. 2007) is a motivation to search for correlations between local environment and internal properties of galaxies. One of this correlation of interest to us, is the possible correlation between λ and environment. Concerning this issue, there are different opposite results. Macció et al. (2007) found an absence of correlation between λ and environment in cosmological simulations, although the opposite was found by other studies using similar techniques (e.g. Avila-Reese et al. 2005,

⁸NGC 5907 has long been used as the prototype of a "noninteracting" warped galaxy. The closest dwarf companion galaxy of NGC 5907 is PGC 54419, which is projected to be only 36.9 kpc from the center of NGC 5907. This dwarf is seen at the tip of the HI warp and in the direction of the warp. Hence, NGC 5907 is then probably interacting with PGC 54419 but not with NGC 5963, too far away

⁹Isolated galaxies are galaxies located in low density environments and selected according to fixed criteria (see Karachentseva 1973; Karachentsev & Petit 1990; Vavilova et al. 2009)

Cervantes-Sodi et al. 2008a,b, 2010a, 2010b). Avila-Reese et al. (2005) employed a Λ CDM N-body simulation to study the properties of galaxy-size dark matter haloes as a function of global environment, where λ was one of the studied properties of the halo, in particular its value in different environments such as clusters, voids or field. Cervantes-Sodi found a marked correlation of λ with mass (Cervantes-sodi et al. 2008a, b), a correlation between λ and cluster environment (Cervantes-Sodi et al. 2010b), and showed that events such as interaction with close neighbors play an important role in the value of the spin for the final configuration (Cervantes-Sodi et al. 2010b). Even the spin alignment of dark matter haloes in different environments, has been studied in some N-body simulations (Aragón-Calvo et al. 2007). From the observational point of view, there has not been much study done on the effects of environment on the slopes of the dark matter halos, simply because the larger samples needed for that do not exist, yet. Hopefully this will change in the next few years, when the LITTLE THINGS (PI: D. Hunter) and VLA-ANGST (PI: J. Ott) will become available, and they should give access to high-resolution HI observations from $\simeq 50$ to 60 dwarf galaxies in various environments. Moreover, THINGS in that respect is a sample that was specifically selected not to contain too many interacting galaxies (apart from one or two show case galaxies), and is therefore not an ideal sample to look at the effects mentioned. Moreover, the techniques actually used to infer the rotation curve makes difficult to address the problem of the quoted correlation. The problem is that when a galaxy is undergoing an interaction, the orbits of the gas particles will change, especially those in the outskirts. So the entire assumption of the gas going around in circular orbits, and the analysis using the ROTCUR approach, will break down. One could, of course, still try to analyze the velocity field and, making some reasonable assumptions, come up with a rotation curve. But if one then find that the inner slope is smaller, there is the problem of how confident can one be in that result: the low value of the slope could be due to the fact that we are fitting a model of circular velocities to what in reality are non-circular motions. One partial solution to the problem would be that of studying dwarfs non strongly interacting with neighbors and to compare with dwarfs in voids or to wait for more sofisticated techniques. Clearly, many work is needed from the theoretical and observational point of view in order to have deeper insights on the role of environment and density profiles of dwarfs and other important questions require further research, including the mechanisms governing dwarf galaxy evolution, and the origin of the morphology-density relation.

4. Conclusions

Using the SIM model introduced in DP09, we studied how the shape of density profiles of dwarfs in the mass range $10^8 - 10^{10} M_{\odot}$ changes when angular momentum originated by

tidal torques, and baryon fraction are changed. As a first step, we calculated the reference density profiles following DP09, plotted in Fig. 1a, then we calculated density profiles of haloes having ordered angular momentum in a range of values compatible with dwarf galaxies haloes and baryon fraction as obtained by McGaugh et al. (2010). We found that density profiles steepen with increasing mass of the halo while increasing angular momentum the density profiles flatten, in agreement with previous works (Sikivie et al. 1997; Avila-Reese et al. 1998; Nusser 2001; Hiotelis 2002; Le Delliou & Henriksen 2003; Ascasibar et al. 2004; Williams et al. 2004). In the case tidal torquing is shut down (zero angular momentum) and baryons are not present, the density profile is very well approximated by an Einasto profile. Increasing baryon fraction one gets flatter profiles. This is due to the fact that when more baryons are present the energy and angular momentum transfer from baryons to DM is larger and DM moves on larger orbits reducing the inner density. We then repeated the same calculations for three dwarfs studied by S03, S05, namely NGC 2976, NGC 5949, and NGC 5963. NGC 2976 has a core profile, NGC 5963 a cuspy profile and NGC 5949 an intermediate one. We calculated the baryon fraction using some assumptions and McGaugh et al. (2010) results and then fitted the rotation curves obtained by S03, S05 with the theoretical curves obtained from our model. NGC 2976 is characterized by a larger value of angular momentum ($\lambda \simeq 0.04$) with respect the other two dwarfs ($\lambda \simeq 0.025$, for NGC 5949; $\lambda \simeq 0.02$, and random angular momentum, j , 1/2 of those of the reference haloes (Fig. 1a), for NGC 5963). Moreover, there are evidences of past tidal interaction between NGC 2976 and M31. Appleton et al. (1981) discovered a faint HI streamer stretching from M81 to NGC 2976, implying an interaction between the two objects, and observations of Williams et al. (2010) showed a process of outer disk gas depletion and inner disk star formation likely triggered by an interaction with the core of the M81 group ≥ 1 Gyr ago. This interaction could be another reason why the density profile of NGC 2976 is so flat. In the case of NGC 5949 and NGC 5963 there is no evidence of this kind of tidal interaction and the closest neighbors are at several hundreds kpc. Concluding, dwarfs galaxies which acquired larger angular momentum by tidal interaction in their formation phase and/or interacted tidally in later phases with neighbors, show a flatter density profile than those who had less tidal interactions.

We would like to thank Josh Simon, Erwin de Blok, Elias Brinks, Benoit Famaey, Alister Graham, Igor Karachentsev, Valentina Karachentseva, and Bernardo Cervantes-Sodi for stimulating discussions on the topics related to the subject of this paper.

- Appleton, P. N., Davies, R. D., & Stephenson, R. J. 1981, MNRAS, 195, 327
- Aragón-Calvo M. A., van de Weygaert R., Jones B. J. T., van der Hulst J. M., 2007, ApJ, 655, L5
- Ascasibar, Y., Yepes, G., & Gottlober, S. 2004, MNRAS, 352, 1109A
- Avila-Reese, V., Firmani, C., & Hernandez, X. 1998, ApJ, 505, 37
- Avila-Reese V., Colin P., Gottlober S., Firmani C., Maulbetsch C., 2005, ApJ, 634,51
- Babul, A., and H. C. Ferguson, H. C., 1996, ApJ 458, no. 1, 100-119.
- Benjamin F. W, et al., 2010, ApJ 709, 135
- Blais-Ouellette, Amram, P., Carignan, C., and Swaters, R., 2004, A&A 420, no. 1, pp. 147-161
- Blumenthal, G. R., Faber, S. M., Flores, R., & Primack, J. R. 1986, ApJ, 301, 27
- Boissier, S., Monnier, R. D., van Driel, W., Balkowski, C., & Prantzos, N. 2003, Ap&SS, 284, 913
- Bolatto, A. D., Simon, J. D., Leroy, A., & Blitz, L. 2002, ApJ, 565, 238
- Borriello, A., & Salucci, P. 2001, MNRAS, 323, 285
- Bothun, D., 1997, AJ 114, no. 5, pp. 1858-1882
- Boyce, P. J., et al. 2001, ApJ, 560, L127
- Broeils, A. H. thesis, Univ. Groningen, 1990.
- Bullock, J. S., et al. 2001, ApJ 555, 240
- Burkert, A. 1995, ApJ, 447, L25
- Carignan, C. & Beaulieu, S., 1989, ApJ. 347, 760-770.
- Catelan, P., & Theuns, T. 1996, MNRAS, 282, 436
- Cervantes-Sodi, B., Hernandez, X., Park, C., Kim, J., 2008a, MNRAS 388, 863
- Cervantes-Sodi, B., Hernandez, X., Park, C., Kim, J., 2008b, RevMexAA (Serie de Conferencias) 34, 87-90
- Cervantes-Sodi, B., Hernandez, X., Park, C., 2010a, MNRAS 402, Issue 3, pages 18071815
- Cervantes-Sodi, B., Park, C., Hernandez, X., Hwang, H. S., 2010b, arXiv:1008.2832
- de Blok W. J. G., and McGaugh, S. S., 1997, MNRAS 290, no. 3, pp. 533-552
- de Blok, W. J. G. 2003, in ASP Conf. Ser. 220, Dark Matter in Galaxies, ed. S. Ryder, et al. (San Francisco, CA: ASP), 69
- de Blok, W. J. G., & Bosma, A. 2002, A&A, 385, 816
- de Blok, W. J. G., 2010, Advances in Astronomy Volume 2010, Article ID 789293, 14 pages
- de Blok, W. J. G., Bosma, A., & McGaugh, S. 2003, MNRAS, 340, 657
- de Blok, W. J. G., McGaugh, S. S., Bosma, A., & Rubin, V. C. 2001, ApJ, 552, L23
- de Blok, W. J. G., Walter, F., Brinks, E., Trachternach, C., Oh, S-H., and Kennicutt, R. C., AJ 136, 2648
- de Naray, R. K., McGaugh, S. S., and de Blok, W. J. G., 2008, ApJ 676, no. 2, pp. 920-943
- de Naray, R. K., McGaugh, S. S., and Mihos, J. C., 2009, ApJ 692, pp. 1321-1332

- Dekel, A., & Woo, J. 2003, MNRAS, 344, 1131
- Del Popolo A., 2009, ApJ 698, 2093-2113
- Del Popolo, A., & Gambera, M. 1996, A&A, 308, 373
- Dressler A., 1980, ApJ, 236, 351
- Duc, P. A., & Mirabel, I. F. 1998, A&A, 333, 813
- Eisenstein, D. J., & Loeb, A. 1995, ApJ, 439, 250
- El-Zant, A., Shlosman, I., & Hoffman, Y. 2001, ApJ, 560, 636
- Ferguson, H. C., Binggeli, B., Astronomy and Astrophysics Review, vol. 6 no. 1-2, 67-122
- Fillmore, J. A., & Goldreich, P. 1984, ApJ, 281, 1
- Flores R., Primack J.R. 1994, ApJ, 427, L1
- Fouqué, P., Gourgoulhon, E., Chamaraux, P., & Paturel, G. 1992, A&AS, 93, 211
- Gao, L., & White, S. D. M. 2007, MNRAS, 377, 5
- Geha M., Blanton2, M. R., Masjedi M. and West, A. A, 2006, ApJ 653, 240
- Gelato, S., and Sommer-Larsen, J., 1999, MNRAS 303, no. 2, pp. 321328
- Gentile, G., Salucci, P., Klein, U., & Granato, G. L. 2007a, MNRAS, 375, 199
- Gentile, G., Salucci, P., Klein, U., Vergani, D., & Kalberla, P. 2004, MNRAS, 351, 903
- Gentile, G., Tonini, C., & Salucci, P. 2007b, MNRAS, 378, 41
- Gnedin, N. Y., and J. P. Ostriker, J. P., 1997, ApJ 486, no. 2, 581-598
- Gnedin, O. Y., Kravtsov, A. V., Klypin, A. A., & Nagai, D. 2004, ApJ, 616, 16
- Governato, F., et al., 2007, MNRAS 374, Issue 4, pp. 1479-1494
- Governato, F., et al. 2010, Nature 463, 203-206
- Grebel, E. K., 2001, in “Dwarf Galaxies and their Environment”, 40th Graduiertenkolleg-Workshop, eds. K.S. de Boer, R.-J. Dettmar, & U. Klein (Bonn:Shaker Verlag), 45-52
- Gunn, J. E. 1977, ApJ, 218, 592
- Gunn, J. E., & Gott, J. R. 1972, ApJ, 176, 1
- Hayashi, E., Navarro, J. F., Taylor, J. E., Stadel, J., & Quinn, T. 2003, ApJ, 584, 541
- Hayashi, E., Navarro, J.F., Power, C., et al., 2004, MNRAS 355, no. 3, pp. 794-812
- Hiotelis, N. 2002, A&A, 383, 84
- Hoefl, M., Yepes, G., Gottlöber, S., Springel, V., 2006, MNRAS 371, no. 1, 401-414
- Hoefl, M. and Gottlöber, S., , Hindawi Publishing Corporation, Advances in Astronomy Volume 2010, Article ID 693968, 16 pages
- Hoffman, Y., & Shaham, J. 1985, ApJ, 297, 16 (HS)
- Hoyle, F. 1949, in IAU and International Union of Theoretical and Applied Mechanics Symposium, Problems of Cosmological Aerodynamics
- Burger & H. C. van der Hulst (Ohio: IAU), 195
- Jaffe, A. H., et al. 2001, Phys. Rev. Lett. 86, 3475
- Jobin, M. & Carignan, C., 1990, AJ 100, 648-662.
- Karachentsev, I. D., and O. G. Kashibadze, O. G., 2006, Astrophysics 49, No. 1

- Karachentsev, I. D., et al. 2002, *A&A*, 383, 125
- Kaufmann et al. 2007, *MNRAS* 375, Issue 1, pages 5367
- Kazantzidis, S., Abadi, M. G., and Navarro, J. F., 2010, *ApJL* 720, L62-L66
- Kleyna, J. T., Wilkinson, M. I., Gilmore, G., & Evans, N. W. 2003, *ApJ*, 588, L21
- Klypin, A., Gottlöber, S., Kravtsov, A. V., & Khokhlov, A.M. 1999, *ApJ*, 516, 530
- Klypin, A., Zhao, H., & Somerville, R. S. 2002, *ApJ*, 573, 597
- Knebe, A., and Power, C., 2008, *ApJ* 678, 621-626
- Kormendy, J., & Kennicutt, R. C. 2004, *ARA&A* 42, 603-683
- Kormendy, J., and Freeman, K. C., 2004, Scaling laws for dark matter halos in late-type and dwarf spheroidal galaxies, in *Dark Matter in Galaxies*, International Astronomical Union Symposium no. 220, pp. 377-397
- Kravtsov, A. V., Klypin, A. A., Bullock, J. S., & Primack, J. R. 1998, *ApJ*, 502, 48
- Kravtsov, A.V., Klypin, A. A., Bullock, J. S., and Primack, J. R., *ApJ* 502, no. 1, pp. 48-58, 1998.
- Le Delliou, M., & Henriksen, R. N. 2003, *A&A*, 408, 27
- Lemson G., Kauffmann G., 1999, *MNRAS*, 302, 111
- Lequeux, J., Combes, F., Dantel-Fort, M., Cuillandre, J. C., Fort, B., Mellier, Y. 1998 *A&AL* 334, L9-L12
- Lilly, S. J., Tresse, L., Hammer, F., Crampton, D., and Le Fèvre, O., 1995, *ApJ* 455, no. 1, pp. 108-124
- Lokas, E. W., Kazantzidis, S., Mayer, L., and Callegari, S., arXiv:1011.3357v1 [astro-ph.CO]
- Magorrian, J. 2003, in *ESO Astrophysics Symposia, The Mass of Galaxies at Low and High Redshift: Proc. ESO Workshop Venice*, ed. R. Bender, A. Renzini (Singapore: Springer), 18
- Flores, R. A., & Primack, J. R. 1994, *ApJ*, 427, L1
- Lake, G., Schommer, R. A. & van Gorkom, 1990, *J. H. AJ* 99, 547-560.
- Maccio A. V., Dutton A. A., van den Bosch F. C., Morre B., Potter D., Stadel J., 2007, *MNRAS*, 378, 55
- Maller, A.H. and Dekel, A.: 2002, *MNRAS* 335, 487.
- Marchesini, D., D’Onghia, E., Chincarini, G., Firmani, C., Conconi, P., Molinari, E., & Zaccari, A. 2002, *ApJ*, 575, 801
- Mashchenko, S., & Sills, A. 2005, *ApJ*, 619, 258
- Mashchenko, S., Couchman, H. M. P., & Wadsley, J. 2006, *Nature*, 442, 539
- McGaugh, S. S., & de Blok W. J. G., 1998, *ApJ* 508, 132
- McGaugh, S. S., Schombert, J. M., de Blok, W. J. G. and Zlagursky, M. J., 2010, 708, L14-L17
- Moore, B. 1994, *Nature*, 370, 629
- Moore, B., Ghigna, S., Governato, F., Lake, G., Quinn, T., Stadel, J., & Tozzi, P. 1999,

- ApJ, 524, L19
- Mun̄oz-Mateos et al. 2011, arXiv:1102.1724v1
- Navarro, J. F., Eke, V. R., and Frenk, C. S., 1996, MNRAS 283, no. 3, pp. L72-L78
- Navarro, J. F., et al. 2004, MNRAS, 349, 1039
- Navarro, J. F., et al. 2010, MNRAS 402, 21
- Nusser, A. 2001, MNRAS, 325, 1397
- Oh, Se-Heon et al. 2010, arXiv:1011.2777
- Ostriker, J.P., Steinhardt, P. 2003, Science, 300, 1909
- Park C., Choi Y., Vogeley M. S., Gott J. R., Blanton M. R., 2007, ApJ, 658, 898
- Peacock, J. A., & Heavens, A. F. 1990, MNRAS, 243, 133
- Peebles, P. J. E. 1969, ApJ, 155, 393
- Peebles, P. J. E. 1980, The Large Scale Structure of the Universe (Princeton, NJ: Princeton Univ. Press)
- Percival. W. J., et al. 2001, MNRAS 327, 1297
- Pickering, T. E., Impey, C.D., van Gorkom, J. H., and Bothun, G. D., 1997, AJ 114, no. 5, pp. 1858-1882
- Ricotti, M., 2009, MNRAS 392, L45-L49
- Romano-Diaz, E., Shlosman, I., Hoffman, Y., & Heller, C. 2008, ApJ, 685, 105
- Ryden, B. S. 1988a, ApJ, 329, 589, (R88)
- Ryden, B. S. 1988b, ApJ, 333, 78
- Ryden, B. S., & Gunn, J. E. 1987, ApJ, 318, 15 (RG87)
- Sales, L. V., Helmi, A., and Battaglia, G., 2010, Advances in Astronomy, Article ID 194345, 14 pages
- Salucci, P., & Burkert, A. 2000, ApJ, 537, L9
- Schaefer, B. M., 2009, Int. J. Modern Phys. D, 18, 173
- Sikivie, P., Tkachev, I. I, & Wang, Y. 1997, Phys. Rev. D, 56, 1863
- Simon, J. D., Bolatto, A. D., Leroy, A., & Blitz, L. 2003, ApJ, 596, 957
- Simon, J. D., Bolatto, A. D., Leroy, A., Blitz, L., and Gates, E. L., 2005 ApJ 621 757
- Simon, J. D., Bolatto, A. D., Leroy, A., & Blitz, L. 2004, in ASP Conf. Ser. 32, Satellites and Tidal Streams, ed. F. Prada, D. Martinez-Delgado, & T. J. Mahoney (San Francisco, CA: ASP), 18
- Spano, M., Marcelin, M., Amram, P., Carignan, C., Epinat, B., and Hernandez, O., 2008, MNRAS 383, no. 1, pp. 297-316
- Spekkens, K., Giovanelli, R., & Haynes, M. P. 2005, AJ, 129, 2119
- Spergel, D. N., Verde, L., Peiris, H. V., et al. 2003, ApJS, 148, 175
- Sprayberry, D., Impey, C. D., Bothun, G. D., and Irwin, M. J., 1995, AJ 109, no. 2, pp. 558-571
- Stadel, J., Potter, D., Moore, B., Diemand, J., Madau, P., Zemp, M., Kuhlen, M., & Quilis,

- V. 2009, MNRAS 398, 21
- Stil, J. M., and Israel, F. P., 2002, A&A 389, 29-41
- Stoehr, F., White, S. D. M., Tormen, G., & Springel, V. 2002, MNRAS, 335, L84
- Swaters, R. A., Verheijen, M. A. W., Bershady, M. A., and Andersen, D. R., 2003, ApJ 587, no. 1, pp. L19-L22
- Swaters, R.A., Madore, B.F., van den Bosch, F. C., and Balcells, M., 2003, ApJ 583, no. 2, pp. 732-751
- Turner, M. S., 2002, ApJ 576, L101–L104
- van den Bosch F. C., Burkert A., Swaters R. A., 2001, MNRAS 326, 1205
- van den Bosch, F.C., Robertson, B.E., Dalcanton, J. J., and de Blok, W.J.G., 2000, AJ 119, no. 4, pp. 1579-1591
- Vitvitska, M., Klypin, A. A., Kravtsov, A. V., Wechsler, R. H., Primack, J. R. and Bullock, J. S., 2002 ApJ 581 799
- White, S. D. M. 1984, ApJ, 286, 38
- White, S. D. M., & Zaritsky, D. 1992, ApJ, 394, 1
- Williams, B. F., et al. 2010, ApJ 709, 135-148
- Williams, L. L. R., Babul, A., & Dalcanton, J. J. 2004, ApJ, 604, 18
- Yun, M. S., Ho, P. T. P., & Lo, K. Y. 1994, Nature, 372, 530
- Zaroubi, S., & Hoffman, Y. 1993, ApJ, 416, 410